Role of substrate outgassing on the formation dynamics of either hydrophilic or hydrophobic wood surfaces in atmospheric-pressure, organosilicon plasmas

O. Levasseur, Luc Stafford, Nicolas Ghérardi, Nicolas Naudé, Eric Bêche, Jérôme Esvan, Pierre Blanchet, Bernard Riedl, Andranik Sarkissian

Role of substrate outgassing on the formation dynamics of either hydrophilic or hydrophobic wood surfaces in atmospheric-pressure, organosilicon plasmas

O. Levasseur [a], L. Stafford [a,*], N. Gherardi [b,c,d,e,f], N. Naudé [b,c,d,e,f], E. Beche [g], J. Esvan [h], P. Blanchet [i], B. Riedl [j], A. Sarkissian [k]

[a] Département de Physique, Université de Montréal, Montréal, QC H3C 3J7, Canada
[b] Université de Toulouse, F-31062 Toulouse Cedex 9, France
[c] UPS, F-31062 Toulouse Cedex 9, France
[d] INPT, F-31062 Toulouse Cedex 9, France
[e] LAPLACE, F-31062 Toulouse Cedex 9, France
[f] CNRS, F-31062 Toulouse Cedex 9, France
[g] PROMES-CNRS/UPR 8521, Centre du four solaire Felix TROMBE, Odeillo, 66120 Font-Romeu, France
[h] CIRIMAT-ENSIACET, 31030 Toulouse Cedex 4, France
[i] FPInnovations – Division des Produits du Bois, Québec, QC G1P 4R4, Canada
[j] Centre de Recherche sur le Bois, Université Laval, Québec, QC G1K 7P4, Canada
[k] Plasmionique, Varennes, QC J3X 1S2, Canada

Keywords:
Atmospheric-pressure plasmas
Dielectric barrier discharges
Functional coatings
Organosilicon plasmas
Wood

A B S T R A C T

This work examines the influence of substrate outgassing on the deposition dynamics of either hydrophilic or hydrophobic coatings on wood surfaces in organosilicon, dielectric barrier discharges. Sugar maple and black spruce wood samples were placed on the bottom electrode and the discharge was sustained in N_2–HMDSO (hexamethyldisiloxane) gas mixtures by applying a 24 kV peak-to-peak voltage at 2 kHz. Current–voltage characteristics revealed a transition from a filamentary to a homogeneous discharge with increasing plasma treatment time, t. Based on optical emission spectroscopy, the filamentary behavior was ascribed to the release of air and humidity from the wood substrate following discharge exposure which produced significant quenching of N_2 metastables. This effect vanished at longer treatment times due to the nearly complete "pumping" of products from the wood substrate and the progressive deposition of a "barrier" layer. Analysis of the surface wettability through static, water contact angles (WCAs) and of the surface composition through Fourier-Transform-Infra-Red-Spectroscopy and X-ray-Photoelectron-Spectroscopy indicated that for $t < 10$ min, the wood surface was more hydrophilic due to the formation of a SiO_x layer, a typical behavior for HMDSO deposition in presence of oxygen. On the other hand, for $t > 10$ min, the static WCA increased up to ~140° due to the deposition of hydrophobic $Si(CH_3)_3$-O-$Si(CH_3)_2$, $Si(CH_3)_3$, and $Si(CH_3)_2$ functional groups.

1. Introduction

Dielectric barrier discharges (DBDs) were thoroughly investigated over the last several years with one of the main goals being the achievement of a homogeneous, or glow, discharge at high operating pressure in various gas mixtures [1–13]. This keen interest is mainly driven by the fact that atmospheric-pressure DBDs present major advantages over low-pressure plasmas for polymer treatments, one of the most important being the ability to work with cold plasmas without the use of high-end and expensive vacuum pumping systems. Over the last decade, many gaseous or liquid precursors, such as organosilicon compounds like hexamethyldisilazane (HMDSN) and hexamethyldisiloxane (HMDSO), were added to these cold, atmospheric-pressure plasmas for plasma-enhanced chemical vapor deposition (PECVD) applications [14]. A wide variety of coatings have been obtained by such PECVD methods, including those relevant for photovoltaic and biomedical applications [15,16]. Application of DBDs to the treatment of textiles and wood is however much more challenging than for conventional substrates such as polymer foil, Si or SiO_2. This can not only be attributed to the highly complex chemical nature of these polymers but also to their generally porous microstructure which can release impurities in the discharge either from plasma–substrate chemical reactions or from sample outgassing (if not pumped-down beforehand). Such impurities can greatly alter the discharge stability and gas-phase kinetics which are both known to play an important role on the plasma deposition dynamics. For example, it is well-known that small admixtures of oxygen in dielectric

* Corresponding author. Tel.: +1 5143436542; fax: +1 5143432071.
E-mail address: luc.stafford@umontreal.ca (L. Stafford).

http://dx.doi.org/10.1016/j.surfcoat.2013.05.045

barrier discharges operated in N_2 lead to a transition from a homogeneous to a filamentary discharge which increases the difficulty of obtaining spatially uniform plasma-deposited layers [17]. In addition, the addition of small amounts of O_2 into a N_2/HMDSO plasma generally leads to the formation of a SiO_x layer instead of the organosilicon coatings obtained in pure N_2/HMDSO discharges [18].

In a previous publication, we have shown that an atmospheric pressure DBD operated in He/HMDSO gas mixtures leads to the deposition of highly hydrophobic functional groups on wood substrates, producing coatings with static, water contact angles in the 130° range and with a high long-term stability following natural weathering, a very promising result for structural and decorative outdoor applications [19]. Other authors have also shown promising hydrophilic or hydrophobic wood surfaces following atmospheric-pressure plasma treatments [see, for example, Refs. 20–23]. In this work, we capitalize on the very porous nature of wood, which can retain a significant amount of impurities, to examine the influence of substrate outgassing during PECVD on the discharge stability and on the evolution of the properties of plasma-deposited thin films.

2. Experimental details

2.1. Experimental setup and plasma diagnostics

The DBD apparatus used in this work was described in details in our previous publication [19]. Briefly, the discharge is sustained into a sealed stainless steel chamber between two 25 × 55 mm metallic electrodes covered with two 0.635 mm thick, 70 × 115 mm alumina sheets. Sugar maple (*Acer saccharum* Marsh.) and black spruce (*Picea mariana* Mill.) samples, 2 mm-thick and 70 × 115 mm in size were placed on the bottom electrode. All samples were cut from the same board and sanded with 80 grit paper before each treatment. The discharge gap between the wood topmost surface and the top electrode was set to 1 mm. All experiments were realized using N_2 (purity grade UHP) as the carrier gas and HMDSO as the growth precursor. The mass flow rate of N_2 was set to 3 SLPM (standard liters per minute at STP) while the HMDSO concentration was set to 20 ppm. For selected samples, a primary vacuum down to about 50 mTorr was performed before the plasma treatment to allow considerable outgassing of the wood substrate and thus to highlight its role on the discharge stability and properties of plasma-deposited thin films. To sustain the plasma, a sinusoidal electrical stimulation with a frequency of 2 kHz and a peak-to-peak voltage of 24 kV was used.

The plasma was characterized through current–voltage (I–V) and optical emission spectroscopy (OES) analysis. The discharge regime was studied by measuring V_a, the voltage applied to the gas, and I_m, the current flowing through the discharge cell [19]. For OES measurements, an optical fiber was installed on the back of the reactor with the tip pointing towards the interelectrode gap. Plasma emissions were analyzed using a PI-Acton spectrometer equipped with a 550 mm focal length monochromator and a Pixis 256E charged-coupled device camera. Emission spectra were taken between 300 and 900 nm with a 300 lines/mm grating. As only the overall evolution of the plasma emission was of interest in this study, the spectra were not corrected by the spectral response of the monochromator and detector.

2.2. Surface characterization

Following plasma exposure, the wettability with deionized water of each sample was characterized by measuring the sessile contact angle, θ, with a Digidrop GBX apparatus. Unless mentioned otherwise, θ values were determined with water drops of 3 μl in volume, 1 s after contact with the wood sample. Because of the strongly inhomogeneous nature of wood in terms of chemical composition and microstructure, at least 10 measurements on different parts of the surface were performed to obtain reliable θ values with minimal standard deviations. As underlined by Strobel and Lyons [24] and by Di Mundo and Palumbo [25], measurements in "static" mode, i.e. by simply placing a drop of liquid on the surface, tend to miss a large part of the available information. Indeed, on non-ideal surfaces such as plasma-modified polymers, measuring both advancing and receding contact angles generally provides a more complete picture of the surface wettability: the advancing contact angle is more sensitive to the low-energy components while the receding contact angle is most sensitive to the high-energy ones. In the present work, however, contact angle measurements were only used to examine whether there was grafting of either hydrophilic or hydrophobic groups on the wood surface following plasma exposure and this aspect can readily be obtained through static measurements. Moreover, in conditions in which the wood surface strongly absorbs the water droplet, receding angles are impossible to determine.

Analysis of the surface chemistry of raw and plasma-treated wood samples was done by Attenuated Total Reflectance Fourier Transform Infrared (ATR-FTIR) spectroscopy in the 700 to 4000 cm^{-1} wavenumber range using a Perkin Elmer (Spectrum 400) apparatus. Each spectrum displayed in this work represents the average of twelve-scans. Since our ATR-FTIR studies only provide qualitative data, the chemical composition of selected wood substrates was also investigated by X-ray Photoelectron Spectroscopy (XPS) using a Thermoelectron Kalpha device from Thermo Scientific. The photoelectron emission spectra were recorded using Al–Kα radiation ($h\nu = 1486.6$ eV) from a monochromatized source and the X-ray spot was approximately 400 μm in size. The pass energy was fixed to 60 eV, the energy step size to 0.1 eV, and the dwell time to 50 ms. The spectrometer energy calibration was made using the Au 4f7/2 (83.9 ± 0.1 eV) and Cu 2p3/2 (932.8 ± 0.1 eV) photoelectron lines. The background XPS signal was removed using the Shirley method. The atomic concentrations were determined with accuracy less than 10% from photoelectron peak areas using the atomic sensitivity factors reported by Scofield, taking into account the transmission function of the analyzer. This function was calculated at different pass energies from Ag 3d and Ag MNN peaks collected for a silver reference sample. The binding energy scale was established by referencing the C 1s value of adventitious carbon (284.6 ± 0.1 eV).

3. Experimental results and discussion

3.1. Role of substrate outgassing on the discharge properties

Fig. 1 shows the discharge current for a sugar maple sample right after ignition of the first few discharges ($t = 0$, Fig. 1A) and after 60 min of plasma exposure ($t = 60$ min, Fig. 1B). Two distinct regions are present on these curves: i) the capacitive current associated with the sinusoidal portion of the electrical signal and ii) the discharge current that can consists of either one broad peak, which is typical of a homogeneous regime, or multiple narrower peaks, which is typical of a filamentary mode [14]. For samples not pumped down beforehand and for short treatment times, the multiple, randomly distributed and intense discharge current peaks of short duration (~100 ns) indicate a strong filamentary behavior. As the wood treatment evolves, the I–Vs show a homogeneous-like behavior characterized by periodic and broad (~80 μs) discharge current peaks. For samples pumped down beforehand (Fig. 1C), the homogeneous regime was observed right after ignition of the first few discharges, which indicates that substrate outgassing plays a very critical role on the discharge stability. The treatment time required to achieve homogeneous I–V characteristics is obviously linked to the nature of the wood samples placed on the electrode since hardwood species are usually less porous than softwood species such that their outgassing time is much longer. As for the power absorbed or dissipated in the discharge, it was found to decrease from 2.5 to 0.8 W cm^{-3} between $t = 0$ and $t = 60$ min, a feature that is in good agreement with

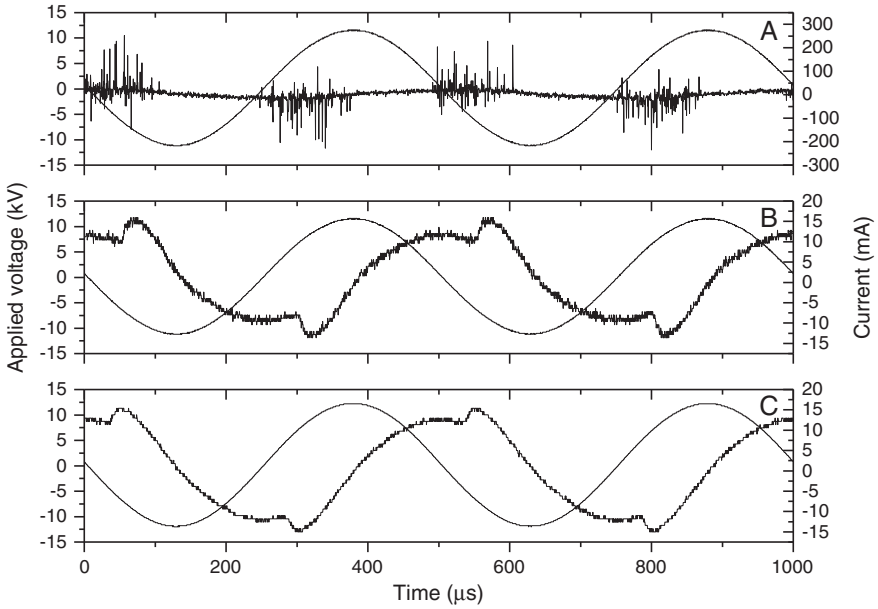

Fig. 1. Comparison of the current-voltage characteristics of a N_2 discharge with a sugar maple sample for various times after ignition of the first few discharges: A) $t = 10$ s and B) $t = 60$ min. Values for outgassed sugar maple samples are also shown for comparison in C). Operating frequency: 2 kHz, peak-to-peak voltage: 24 kV.

the filamentary-to-homogeneous regime transition (filamentary discharges are characterized by higher absorbed powers than those in the homogeneous regimes [26,27]).

Optical emission spectroscopy was performed to examine in more details the impact of wood presence on the plasma properties. A typical emission spectrum from a N_2 discharge with 20 ppm of HMDSO and a sugar maple sample placed on the bottom electrode is shown in Fig. 2. In addition to the expected strong emission from the second positive of N_2 ($C_3\Pi_u$-$B_3\Pi_g$) in the 300–600 nm range, emissions from the fist negative system of N_2^+ at 391 nm ($B^2\Sigma_u^+$, $\nu' = 0 \rightarrow X_2\Sigma_g^+,\nu'' = 0$) and from the $A^2\Sigma^+,\nu' = 0 \rightarrow X^2\Pi,\nu'' = 0$ rovibronic band of OH at 309 nm can also be observed. The release of oxygen-based products (as illustrated by the presence of the OH emission) in the nominally pure N_2–HMDSO discharge can be ascribed to both the strong outgassing of air (N_2 and O_2) and humidity entrapped in the wood substrate as well as to etching of the wood major components (cellulose, hemicelluloses and lignin). This is likely to be responsible for the filamentary behavior displayed in Fig. 1. As reported in [5,26,28], homogeneous or glow discharges can be attained by high metastables and seed electron densities. However, as oxygen impurities are introduced in the discharge, much higher collisional quenching rates and thus lower number densities of N_2 metastables are expected, which is known to lead to a filamentary discharge for O_2 rate in N_2 higher than 500 ppm [29]. In contrast to Ref. [14], it is worth mentioning that no CN emission was observed at 388 nm. This could happen when an oxidizing gas (O_2, humidity) is introduced in the gas phase. It could also suggest that the association rate of HMDSO and N_2 fragments in the plasma was relatively low; a feature that can probably be ascribed to the relatively low dissociation levels of both HMDSO and N_2 in the range of experimental conditions investigated.

Fig. 3 shows the time evolution of the OH, N_2 and N_2^+ emission bands at 309, 337 and 391 nm respectively for sugar maple and black spruce samples exposed to a nitrogen discharge. The emission from N_2 was found to remain fairly constant over the whole

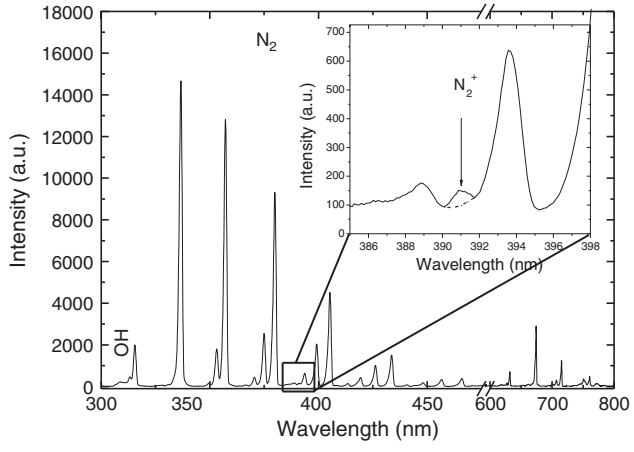

Fig. 2. Typical time- and line-integrated plasma emission spectrum from a N_2 discharge with a non-degassed sugar maple substrate. A zoom over the 390 nm wavelength range is also presented to better illustrate the N_2^+ emission band at 391 nm. As illustrated, for this N_2^+ band, the contribution from surrounding N_2 bands to the emission intensity was removed using a simple linear baseline. The operating conditions are the same than in Fig. 1A.

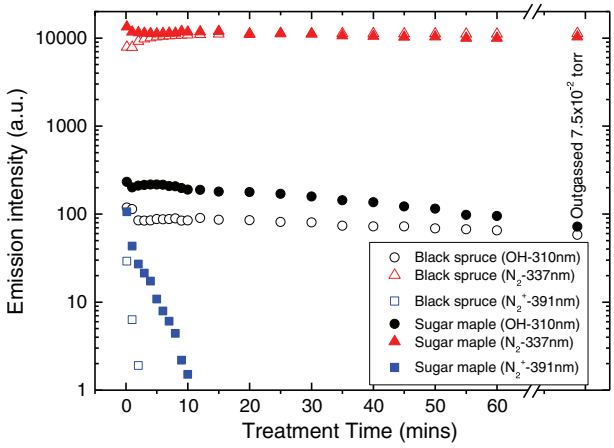

Fig. 3. Influence of treatment time on the intensity of the OH (309 nm), N_2–C (337 nm) and N_2^+ (391 nm) emission bands in a N_2 discharge for sugar maple and black spruce wood samples. Values for outgassed sugar maple samples are also shown for comparison. Operating conditions are the same than in Fig. 1.

60-minute exposure examined whereas the emission from N_2^+ decreased drastically within the first few minutes and vanished completely at longer treatment times. While emission from N_2^+ is generally very weak in homogenous and nominally pure N_2 discharges, it becomes more apparent in the presence of small admixtures of O_2 due to the filamentary-to-homogeneous regime transition [30]. Even if emission from O and O_2 could not be observed in any of the emission spectra, the combination of a filamentary discharge (Fig. 1) and a relatively high N_2^+ emission at short treatment times (Fig. 3) appear strongly linked to a high oxygen content in the discharge. As wood outgassing evolves, i.e. as O_2 and humidity are being pumped down from the substrate, the discharge becomes homogeneous and N_2^+ emission becomes very small. A faster decrease of the N_2^+ emission was observed for black spruce than for sugar maple.

Fig. 4 shows the N_2^+ (391 nm)-to-N_2 (337 nm) and OH (309 nm)-to-N_2 (337 nm) intensity ratios for sugar maple samples exposed to pure N_2 plasma and N_2/HMDSO (20 ppm) plasmas. As a consequence of the decrease in O_2 content and regime transition, the N_2^+-to-N_2 ratio decreased with increasing plasma exposure time, going from 0.008 right after ignition of the first few discharges to 0 in about 10 min. A faster decrease was observed with 20 ppm of HMDSO, indicating that the growth of a thin layer on the plasma-exposed topmost surface prevents the release of air and humidity entrapped in the wood substrate. The OH-to-N_2 ratio also decreased with treatment time in N_2 although the decrease was slower than for the N_2^+-to-N_2. In addition, the OH-to-N_2 ratio for samples pumped down to 50 mTorr (~0.007) was comparable to the one measured for $t = 60$ min (~0.009), indicating that surface etching of the wood components which is expected to release significant amounts of OH remains important independently of wood outgassing effects. On the other hand, with 20 ppm of HMDSO, the decrease of OH/N_2 with t was much more drastic than in pure N_2, reaching the same 0.009 ratio in under 5 min and 0.005 after 60 min. This result is again ascribed to the deposition of a thin "barrier" layer preventing etching reactions.

3.2. Role of substrate outgassing on surface wettability

Fig. 5 compares the dynamic water contact angles of sugar maple samples exposed to a N_2 plasma with 20 ppm HMDSO for 1 and 60 min with those obtained right after sanding. Dynamic water contact angles for samples outgassed prior to plasma exposure are also shown for comparison. All data were recorded as a function of time following the contact between the water droplet and the wood surface. As expected, freshly-sanded wood surfaces exhibited a highly hydrophilic behavior with the water droplet being completely absorbed within a few seconds; a result that is in good agreement with those reported in [31]. For $t = 60$ min, both the as-received and pumped-down samples showed a hydrophobic behavior with static contact angles in the 140° range. Major difference arises when comparing the samples treated for 1 min. For samples pumped down, the WCA were in the same range as the samples treated for 60 min whereas those that were not outgassed beforehand exhibited a more complex time behavior: the WCA first rapidly decreased with a decay rate comparable to those of freshly-sanded samples and then decreased more slowly, going from ~50° to ~40° in about 25 s. This suggests that outgassing of the sample during such short treatment time leads to a more hydrophilic SiO_x-like layer rather than the more hydrophobic organosilicon layer expected from deposition in pure N_2–HMDSO discharges [18]. As for the "two-rate" time behavior, it can probably be ascribed to the non-conformity of the coating as a result of both the short treatment time and the high roughness (even after sanding) of wood surfaces.

The water contact angle at 1 s after the water drop is presented in Fig. 6 as a function of treatment time for sugar maple and black spruce samples exposed to N_2 discharges with 20 ppm of HMDSO. For outgassed samples, similar WCAs were obtained for t ranging from 1 to 60 min for both wood species. The deposition rate in such conditions was roughly estimated by measuring the coating thickness using a KLA-Tencor Alpha-Step IQ profiler. Wood surfaces being too irregular to obtain reliable thicknesses, measurements were performed on a thick glass plate exposed to the same operating conditions with the same mean absorbed power of 1.0 W cm^{-3} in order to get an order of magnitude of the deposited thickness. A deposition rate of about 15 nm/min was obtained. The results presented in Fig. 4 thus indicate that even coatings with thicknesses which are much lower than the wood roughness (for example, of about 15 nm for $t = 1$ min.) can produce high static WCA. On the other hand, for samples not outgassed beforehand, the WCA increased from ~50° for $t = 1$ min to ~140° for $t = 60$ min. As mentioned earlier and shown below, this behavior can be ascribed to the wood outgassing which modifies the chemical composition of the plasma-deposited layer. As wood outgassing evolves, WCA values approach those expected for deposition in nominally pure N_2/HMDSO discharges. WCA measurements being surface sensitive, virtually seeing only the first monolayer of the substrate, high contact angles can be obtained at long treatment times even if the first few monolayers deposited on the topmost wood surface could be more hydrophilic. In the case of black spruce, a less prominent increase was observed, with the WCA going from ~125° for $t = 4$ min to 140° for $t =$ 60 min. This result is consistent with the quicker outgassing time of this wood species underlined from the analysis of the emission

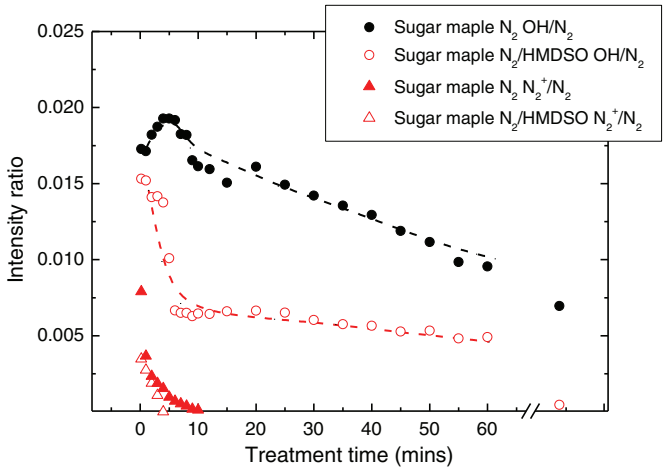

Fig. 4. N_2^+-391 nm-to-N_2-337 nm bandhead intensity ratio and OH-309 nm-to-N_2-337 nm bandhead intensity ratio as a function of exposure time to either a N_2 or N_2/HMDSO (20 ppm) discharge with a non-degassed sugar maple substrate.

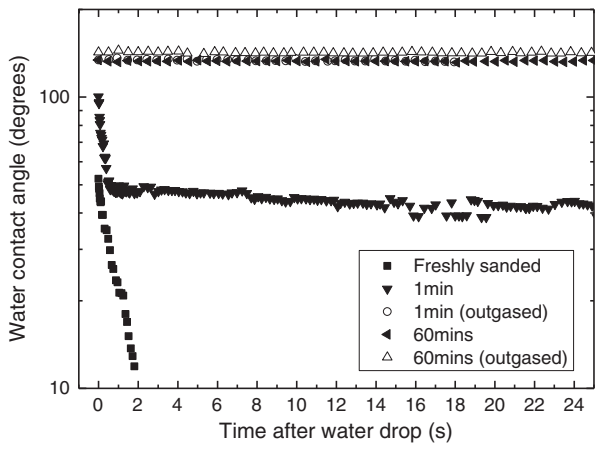

Fig. 5. Dynamics of the wetting process on sugar maple wood samples exposed to N_2\HMDSO (20 ppm) plasmas for times ranging from 1 to 60 min. WCAs from freshly-sanded sugar maple are also shown for comparison.

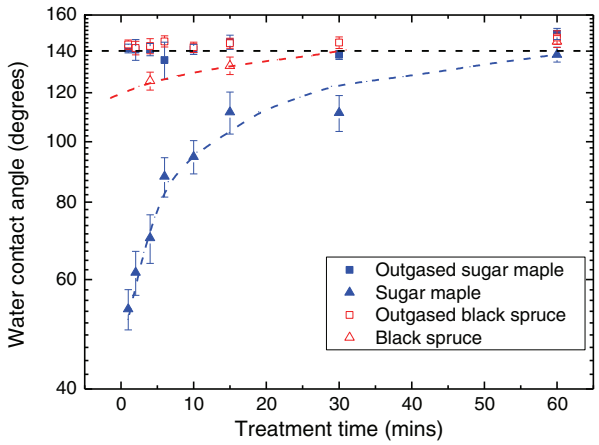

Fig. 6. Influence of the plasma exposure time on the WCA for sugar maple and black spruce wood samples exposed to N_2/HMDSO (20 ppm) plasmas. Operating conditions are the same than in Fig. 1.

spectra (Fig. 3). It is worth mentioning that for samples not outgassed beforehand, a non-linear deposition rate is expected due to the evolving discharge characteristics in regards to sample outgassing. Therefore, an absolute thickness value of the hydrophilic or hydrophobic coating deposited on wood cannot simply be estimated from measurements of the deposition rates on glass samples as these samples are not subjected to the same outgassing effects.

3.3. Role of substrate outgassing on surface chemistry

To demonstrate the role of wood outgassing on the evolution of the chemical composition of the plasma-deposited layers obtained in N_2 discharge with 20 ppm of HMDSO, ATR-FTIR analysis was performed on selected wood samples. Fig. 7 compares the normalized ATR-FTIR spectra as a function of treatment time for sugar maple samples pumped down to about 50 mTorr before plasma exposure. A spectrum from a non-treated, freshly-sanded sample is also shown for comparison. The main visible features in the 3400 cm^{-1} region corresponds to the O–H stretching mode while those in the 1800 cm^{-1} to 900 cm^{-1} range can be attributed to the wood's main constituents, namely cellulose, hemicelluloses and lignin which are essentially composed of C–O, C═C, C–H and C═O groups [32,33]. For $t = 1$ min, the spectrum is very similar to the raw spectrum due to the expected very low thickness of the plasma-deposited layer. For longer treatment times, there is a sharp increase in the signal from

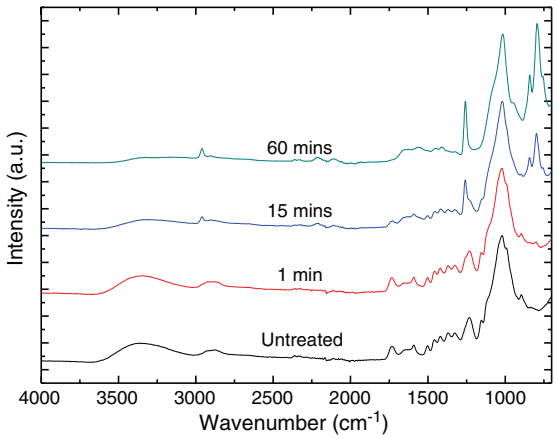

Fig. 7. Influence of the plasma exposure time on the ATR-FTIR spectra for outgassed sugar maple samples exposed to N_2/HMDSO (20 ppm) plasmas. The spectrum of untreated sugar maple is also shown for comparison. The normalization was done using the C–O band at approx. 1018 cm^{-1}. Operating conditions are the same than in Fig. 1.

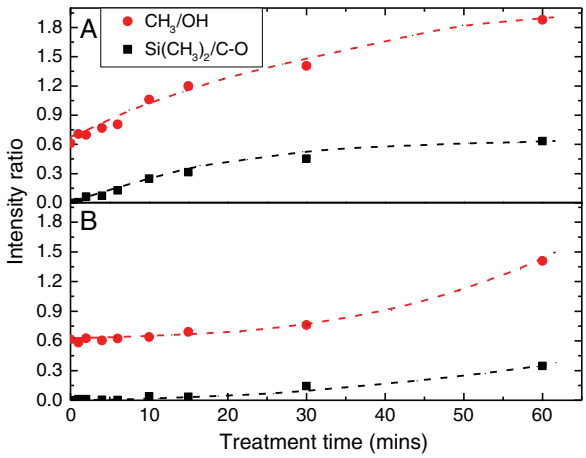

Fig. 8. Influence of treatment time on intensity ratio of $Si(CH_3)_2$ (800 cm^{-1}), CH_3 (2960 cm^{-1}) and OH (3350 cm^{-1}). ATR-FTIR bands for A) an outgassed sugar maple sample and B–C) a non-outgassed sugar maple sample. Operating conditions are the same than in Fig. 1.

hydrophobic functional groups such as CH_x in the 2900 cm^{-1} region as well as Si-$(CH_3)_{2,3}$ at 800 and 840 cm^{-1}. Moreover, there is a visible broadening of the 1230 cm^{-1} band leading to a single band at 1259 cm^{-1} for the 60-minutes deposited sample. This result can be attributed to the apparition of a new absorption band due to Si–C stretching in $Si(CH_3)_2$ and a decrease in wood's main features as the thickness of the plasma-deposited coating increases.

Fig. 8 compares the influence of treatment time on the $Si(CH_3)_2$-to-CO and CH_x-to-OH band intensity ratios for outgassed (Fig. 8A) and non-outgassed (Fig. 8B) samples exposed to the same discharge conditions. The prompt augmentation of the hydrophobic features like $Si(CH_3)_x$ and CH_x over the wood's natural hydrophilic features OH and CO is consistent with the highly hydrophobic behavior deduced from dynamic WCA measurements and from the quasi-linear increase of the coating thickness with plasma exposure time. On the other hand, for samples not-outgassed prior to plasma exposure, the $Si(CH_3)_2$-to-CO and CH_x-to-OH band intensity ratio remained quasi constant within the first few minutes due to the important concentration fraction of wood hydrophilic groups; a feature that is consistent with the high wettability reported above for such surfaces. At longer treatment times, both ratios sharply increased, in good agreement with the prominent increase of the WCA displayed in Fig. 6.

Since ATR-FTIR studies only provide relative information on the surface composition, a quantitative investigation was performed through XPS measurements. Table 1 shows the atomic concentration fraction (in %) of C, O, N and Si for sugar maple samples exposed to N_2–HMDSO (20 ppm) discharges for t ranging from 5 to 60 min. Values for untreated and outgassed samples are also shown for comparison. A drastic decrease of the carbon concentration together with an important increase of the Si, N, and O concentration was observed at short treatment times. As wood outgassing evolves, i.e. for longer treatment times, the C concentration increased, the O concentration decreased, and the N concentration increased, while the concentration

Table 1
Influence of the treatment time, t, on the atomic composition (at.%) of sugar maple samples treated in a N_2–HMDSO discharge. Measurements were performed immediately after the plasma treatment. Values for untreated and outgassed samples are shown for comparison.

Element	Untreated	5 min	15 min	30 min	60 min	Outgassed
C1s	77.3	18.7	19.8	33.2	37.7	52.0
O1s	20.6	48.9	47.9	35.4	30.4	19.7
N1s	Trace	2.5	1.4	2.8	4.5	5.3
Si2p	0	29.9	30.9	28.6	27.4	18.6

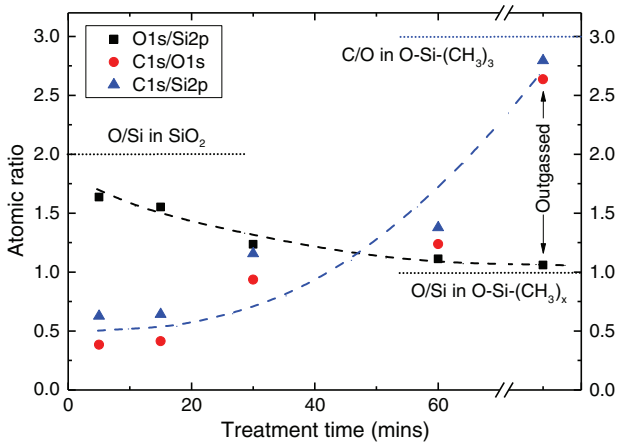

Fig. 9. Influence of treatment time on atomic concentration ratios of O-to-Si, C-to-O and C-to-Si obtained by XPS analysis for samples exposed to N_2/HMDSO plasmas. Operating conditions are the same than in Fig. 1.

of Si remained more or less constant. These results are consistent with our ATR-FTIR observations indicating that substrate outgassing leads to a more SiO_x-like layer that shifts towards $Si(CH_3)_x$ at longer plasma exposition times when outgassing effects are less important. This feature is better illustrated in Fig. 9 that shows the O-to-Si, C-to-O and C-to-Si atomic concentration ratios deduced from the data displayed in Table 1 as a function of plasma deposition time. For $t = 5$ min, the O-to-Si ratio was 1.6, which is close to the composition of the highly hydrophilic SiO_2 coating. This ratio decreased down to about 1, the value expected for deposition of large O-Si-$(CH_3)_3$ fragments (equal amount of Si and O). As for the C-to-Si and C-to-O, both atomic composition ratios varied similarly, going from about 0.5 for $t = 5$ min to about 1.5 for $t = 60$ min. The values are however lower than those of the C-to-Si and C-to-O ratios of about 3 achieved for samples outgassed beforehand and consistent with the deposition of O-Si-$(CH_3)_3$ groups. The lower C-to-Si and C-to-O values obtained without prior outgassing of the wood samples indicates that small amounts of oxygen-based products remain in the gas-phase even after 60 min of discharge exposure and that these species still contribute to the removal of carbon groups from the coating. Similar atomic ratios were obtained on black spruce surfaces (not shown), although the decrease of the O-to-Si and increase of the C-to-Si and C-to-O were, as expected, more rapid.

4. Conclusion

In summary, the objective of this work was to examine the influence of substrate outgassing on the deposition dynamics of hydrophilic or hydrophobic functional groups on sugar maple and black spruce wood substrates exposed to atmospheric-pressure dielectric barrier discharges in N_2–HMDSO gas mixtures. Electrical characterization of the discharge revealed a transition from a filamentary to a homogeneous regime and a decrease of the absorbed power with increasing plasma treatment time. For samples outgassed beforehand, the discharge was homogeneous independently of plasma exposure time. Optical emission spectroscopy showed fairly constant emission from N_2 and a decrease of OH and N_2^+ emissions with t. Change in the discharge stability and plasma emission properties were ascribed to outgassing of air and humidity from the wood substrates. Outgassing effects were found to vanish with time due to the nearly complete "pumping" of free air and humidity entrapped in wood and the progressive deposition of an organosilicon "barrier" layer. Surface wettability of the plasma-deposited coatings was examined through water contact angles and revealed the formation of highly hydrophobic wood surfaces. However, for short deposition times, the surfaces remained hydrophilic due to the formation of SiO_x layer. Such feature is typical for HMDSO deposition in the presence of small admixtures of oxygen. In our case, however, oxygen was injected in the gas phase involuntarily due to substrate outgassing. Future studies should examine whether the presence of such "interfacial" SiO_x layer during growth of hydrophobic organosilicon coatings in N_2/HMDSO discharges helps or deteriorates the adherence and long-term dimensional stability of the coatings.

Acknowledgments

This work was supported by the National Science and Engineering Research Council (NSERC), the Fonds de Recherche du Québec – Nature et Technologies (FRQNT) and the Association Nationale de la Recherche (ANR). The authors would also like to acknowledge the financial contribution of the Commission Permanente de Coopération Franco-Québécoise (CPCFQ) through the Samuel de Champlain program, the Direction des Relations Internationales of the Université de Montréal, and the Région Midi-Pyrénées.

References

[1] S. Kanazawa, et al., J. Phys. D Appl. Phys. 21 (1988) 838–840.
[2] F. Massines, et al., Eur. Phys. J. Appl. Phys. 47 (2) (2009) 22805.
[3] H. Luo, et al., Appl. Phys. Lett. 91 (22) (2007) 221504.
[4] K.V. Kozlov, et al., J. Phys. D Appl. Phys. 38 (4) (2005) 518–529.
[5] A. Sublet, et al., Plasma Sources Sci. Technol. 15 (4) (2006) 627–634.
[6] F. Massines, et al., J. Appl. Phys. 83 (6) (1998) 2950–2957.
[7] B. Eliasson, U. Kogelschatz, IEEE Trans. Plasma Sci. 19 (2) (1991) 309–323.
[8] U. Kogelschatz, B. Eliasson, W. Egli, J. Phys. IV 07 (C4) (1997), (C4-47-C4-66).
[9] U. Kogelschatz, Plasma Chem. Plasma Process. 23 (1) (2003) 1–46.
[10] B. Eliasson, U. Kogelschatz, J. Phys. B: At. Mol. Phys. 19 (8) (1986).
[11] U. Kogelschatz, IEEE Trans. Plasma Sci. 30 (4) (2002) 1400–1408.
[12] M. Šimor, et al., Appl. Phys. Lett. 81 (15) (2002) 2716.
[13] D. Braun, U. Kuchler, G. Pietsch, J. Phys. D: Appl. Phys 24 (4) (1991).
[14] D. Trunec, et al., J. Phys. D: Appl. Phys. 37 (15) (2004) 2112–2120.
[15] L.-B. Di, et al., J. Phys. D: Appl. Phys. 42 (3) (2009) 032001.
[16] P. Favia, R. d'Agostino, Surf. Coat. Technol. 98 (1998) 1102–1106.
[17] R. Brandenburg, et al., J. Phys. D: Appl. Phys. 38 (11) (2005) 1649–1657.
[18] K. Schmidt-Szalowski, et al., Plasma Polym. 5 (3/4) (2000) 173–190.
[19] O. Levasseur, et al., Plasma Processes Polym. 9 (11–12) (2012) 1168–1175.
[20] R. Mahlberg, et al., Int. J. Adhes. Adhes. 18 (1998) 283–297.
[21] A.R. Denes, et al., Holzforschung 53 (1999) 318–326.
[22] G. Avramidis, et al., Wood Mater. Sci. Eng. 4 (1–2) (2009) 52–60.
[23] M. Odraskova, et al., 28th ICPIG, Institute of Plasma Physics AS CR, v.v.i., Prague, Czech Republic, July 15-20 2007.
[24] M. Strobel, C.S. Lyons, Plasma Processes Polym. 8 (1) (2011) 8–13.
[25] R. Di Mundo, F. Palumbo, Plasma Processes Polym. 8 (1) (2011) 14–18.
[26] N. Gherardi, et al., Plasma Sources Sci. Technol. 9 (2000) 340–346.
[27] N. Naudé, et al., J. Phys. D: Appl. Phys. 38 (4) (2005) 530–538.
[28] F. Massines, et al., Surf. Coat. Technol. 174–175 (2003) 8–14.
[29] R. Brandenburg, et al., J. Phys. D: Appl. Phys. 38 (13) (2005) 2187–2197.
[30] A. Fridman, A. Chirokov, A. Gutsol, J. Phys. D: Appl. Phys. 38 (2) (2005) R1–R24.
[31] A. Wolkenhauer, et al., Int. J. Adhes. Adhes. 29 (1) (2009) 18–22.
[32] A. Awal, M. Sain, J. Appl. Polym. Sci. 122 (2) (2011) 956–963.
[33] K.K. Pandey, J. Appl. Polym. Sci. 71 (1999) 1969–1975.